Fabrication of high-density and translucent Al-containing garnet, $Li_{7-x}La_3Zr_{2-x}Ta_xO_{12}$ (LLZTO) solid-state electrolyte by pressure filtration and sintering

Chong Lei, Dinesh Shetty, Michael F. Simpson*, and Anil Virkar
Department of Materials Science & Engineering, University of Utah, 122 S. Central Campus Dr., #304, Salt Lake City, UT 84112
*corresponding author (michael.simpson@utah.edu)

Kewords: solid state electrolyte, batteries, lithium, LLZTO

Abstract

Garnet type LLZTO ceramic oxide is a promising solid-state electrolyte for use in Li-ion batteries because it has good chemical stability, adequate mechanical strength. However, lithium dendrite growth still needs to be addressed. The opacity of the solid electrolyte hinders in-situ investigation of dendrite growth. Therefore, semi-transparent LLZTO with high-density is needed. The traditional fabrication process for the garnet type LLZTO is cumbersome, and dense LLZTO disks with high transparency are difficult to fabricate. In this work, Al-LLZTO powder was made by solid-state reaction. A wet ceramic processing method, pressure filtration followed by sintering, was developed to make dense LLZTO with high ionic conductivity (1.47×10^{-4} S/cm) and adequate transmittance (17–23%) to visible light from 500 to 800 nm to observe and monitor dendrite growth.

1. Introduction

With the increasing demand for energy storage devices under ambient pressure, extensive battery technology development is underway. Lithium-ion batteries (LIBs) are currently of great interest due to their high energy density and long cycle life [1,2]. However, current LIBs have some safety problems because of the flammable organic electrolyte used, and battery failures can contribute to dangerous fires. Solid-state LIBs with wide electrochemical potential working windows are drawing attention since they are stable, durable, non-flammable, and have high mechanical integrity [1,3,4]. Because of the safety benefits, solid-state electrolytes are potential options to

replace the traditional organic electrolyte in LIBs. Recently, a garnet-type oxide ceramic, $Li_7La_3Zr_2O_{12}$ (LLZO), exhibiting good performance in LIBs with high lithium-ion conductivity ($>10^{-4}$ S/cm) at room temperature has been developed [5]. LLZO has two crystal phases, a cubic garnet phase and a tetragonal garnet phase. The cubic garnet phase is more of interest, since it has two orders of magnitude higher Li-ion conductivity than the tetragonal LLZO [6,7]. In order to form the cubic garnet phase and increase the ionic conductivity, various elements are used as dopants, including Ga, Ta, Mg, and Nb. Ta is considered to be a promising dopant to achieve high lithium-ion conductivity in a composition, $Li_{7-x}La_3Zr_{2-x}Ta_xO_{12}$ (Ta-doped LLZO) [8,9]. Low doping level is preferred, since high ionic conductivity can be achieved with a lower cost. In this work, materials were studied with a target doping level of x=0.25. Thus, LLZTO in this work refers to $Li_{6.75}La_3Zr_{1.75}Ta_{0.25}O_{12}$ (LLZTO).

Previous research has focused on enhancing the ionic conductivity of garnet-type oxide ceramics. However, the transparency of these ceramics is seldom reported. A Mg-doped LLZO with 10-12% transparency from 500-800 nm was reported by Yang et al. [10]. The transparency of LLZO with other dopants still needs to be studied. The opacity of the solid electrolyte hinders in-situ investigation of lithium dendrite growth. In this work, translucent LLZTO solid electrolyte was developed, which opens a new opportunity to investigate lithium dendrite growth. High-temperature, atmosphere sintering or cumbersome fabrication processes are usually required to obtain high-quality LLZTO [11–13]. Unlike traditional dry processing methods for ceramics, colloidal processing techniques such as slip casting, gel casting and pressure filtration followed by sintering are considered to be good methods to prepare uniform, high-density ceramics with high transmittance [14–16]. Dasgupta et al. [17] obtained translucent $Al_{2-x}Sc_x(WO_4)_3$ disks by using slip-casting and sintering. Research by Wen and Shetty showed that transparent alumina disks can be obtained by colloidal processing and sintering [18]. Among the colloidal processing techniques, pressure filtration followed by sintering is one of the simplest since it can reduce the consolidation time and enhance density [19,20]. Therefore, in this work, pressure filtration was developed as a simple method for the fabrication of Ta-doped LLZO ($Li_{6.75}La_3Zr_{1.75}Ta_{0.25}O_{12}$).

2. Experimental details

A solid-state method was used for the synthesis of Al containing $Li_{6.75}La_3Zr_{1.75}Ta_{0.25}O_{12}$ powders (Al-LLZTO). Stoichiometric amounts of $LiOH \cdot H_2O$, (Sigma-Aldrich, 99.0%), La_2O_3 (Alfa Aesar, 99.99%, calcined at 900°C for 12 h before using), ZrO_2 (Sigma-Aldrich, 99.0%), Ta_2O_5 (Sigma-Aldrich, 99.99%), and Al_2O_3 (Alfa Aesar, 99.9% - 0.15 mol per mol LLZTO) were planetary milled in 2-propanol for 8h. Excess of 15wt% LiOH was added to compensate for lithium loss during sintering. Al_2O_3 was added as a sintering aid to stabilize the cubic garnet phase and enhance density [7,9,21]. The powder was then dried and calcined at 900°C for 6h. The as-calcined powder was planetary milled in 2-propanol for 13h. The milled slurry was dried and then ground by mortar and pestle. Al-LLZTO suspensions in water were made with 50 and 70wt% of solids. In order to minimize flocculation, 0.1 mg/m^2 of dispersant (DARVAN C-N, Vanderbilt Minerals LLC, Norwalk, CT) was added to the suspensions. The suspensions were ultrasonicated to breakdown soft agglomerates. Disk-shaped green compacts of Al-LLZTO were consolidated with 50wt% and 70wt% suspensions by pressure filtration. Figure 1 shows a schematic of the pressure filtration device in which the garnet suspension was placed between the Teflon disk and the filter paper [22]. A pressure of 20 MPa was applied for 10 minutes during filtration. The disks were dried at 100°C in a muffle furnace for 2 days before sintering. The dried disks were buried in the mother powder in alumina crucibles covered with alumina lids to minimize loss of volatile components. Samples were sintered at 1100, 1140, and 1180°C for 4h in air. Dry-pressed disks were also made by uniaxial pressing dry powders and sintering under the same conditions as the filter-pressed disks.

The particle size distribution of the Al-LLZTO powder was analyzed using a particle size analyzer (Beckman Coulter LS230) with distilled water as the medium. The specific surface area of Al-LLZTO ground powders was measured and calculated by BET (Micromeritics Gemini V). XRD patterns of the sintered disks were obtained using an X-ray diffractometer (Bruker D2 Phaser) with Cu kα radiation to determine the phases present in the sintered Al-LLZTO disks. Some sacrificial disks were cut through the thickness, ground, polished and thermally etched in air at a temperature 50 degrees below the corresponding sintering temperature for characterization of microstructures using a scanning electron microscope (FEI Nova Nano SEM 630). Densities of the sintered disks were measured using the Archimedes method with ethanol as the immersion fluid. The theoretical density of Al-LLZTO is 5.25 g/cm^3 which was derived from the lattice parameter in the Pearson's Crystal Database (Pearson's crystal data card #1022598). The relative

density was calculated as a ratio of the measured density and the theoretical density. The dry weight before density measurement was measured, and the weight after immersion in ethanol (surface wiped dry) was also measured. The weight increase was calculated to determine if there is any open connected porosity in the Al-LLZTO disks. The ionic conductivities of the sintered disks were measured by electrochemical impedance spectroscopy (EIS) with a Solartron electrochemical interface (SI 1287) and an impedance/gain-phase analyzer (SI 1260) using a 2-probe method. Gold paste was applied symmetrically on both surfaces of the sintered disks as electrodes and fired at 500°C for 1h. The range of frequencies used was from 100 Hz to 1 MHz, with an amplitude of 10 mV, and a temperature range from room temperature to 80°C. All disks were ground down to the same thickness, and surface polished before transmittance measurement. The surface roughness (Rz) was measured by a surface profile gauge (Dlteren SRT-6223+). Transmittance profile of sintered disks was measured with a UV-vis-spectrum (Perkin Elmer Lambda 950 UV-Vis-NIR), from 300 to 800 nm.

A lithium dendrite growth experiment was conducted on a sintered AlLLZTO disc made by pressure filtration followed by sintering. A lithium wire was placed on the disc and a silver wire was also placed. The assembly was placed inside an argon-filled glove box. A DC voltage was applied the two wires to observe any possible dendrite growth.

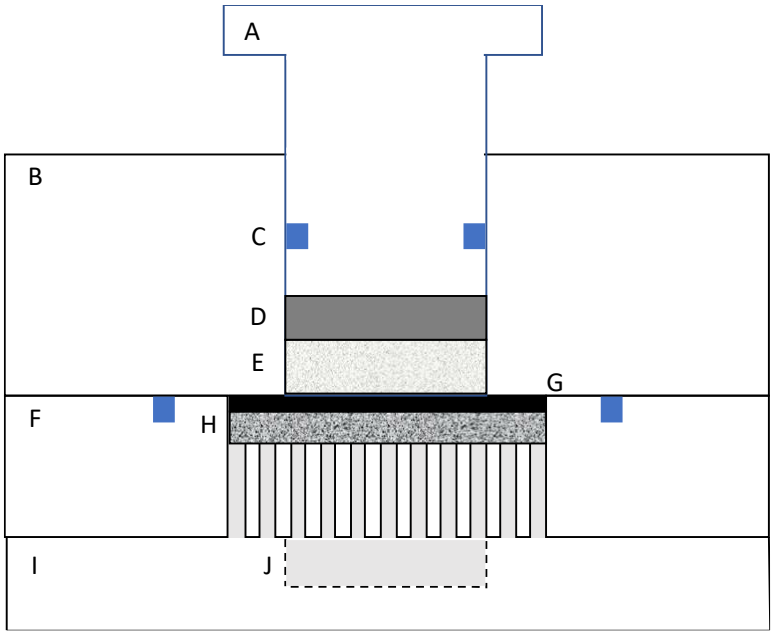

Fig. 1. Schematic of the pressure filtration device. A: cylinder, B: bore plate, C: o-ring, D: Teflon disk, E: garnet suspension, F: filter plate, G: filter paper, H: porous metal disk, I: drain plate, J: outlet for the filtrate [22].

3. Results and discussion

Small particle size, narrow size distribution and stable dispersions are required to obtain low viscosity suspensions at high solids content [23,24]. Large agglomerates contribute to high viscosity of the suspension, which makes them unstable [16]. Figure 2 shows the particle size distribution of the Al-LLZTO powder before and after grinding by mortar and pestle. Before grinding by mortar and pestle, there are four peaks in the particle (agglomerate) size distributions at about 0.6, 3.5, 15, and 40 µm, and the particle size range is from 0.06 to 80 µm. About 40v% of the particles are larger than 10 µm. After grinding by mortar and pestle, there are two peaks, one at about 0.3 µm and the other at about 1.8µm, and the particle size range is from 0.04 to 10 µm. About 28v% of the particles are smaller than 0.3 µm, and about 78v% of the particles are smaller than 1.8 µm. Grinding by mortar and pestle breaks almost all of the agglomerates larger than 10 µm, and some agglomerates smaller than 10 µm, which also makes the particle size distribution narrower. The BET specific surface area was 4.06 and 8.44 m^2/g, before and after grinding,

respectively. The particle distribution of the powder is important, because the dispersant added into the suspension can help maintain particles smaller than 10 μm and prevent flocculation. In order to obtain green bodies with high and uniform density, flocculation of particles must be avoided, since it can affect the consolidation of particles, and leads to green bodies with low packing density [19]. Therefore, powders were ground by mortar and pestle before pressure filtration or dry pressing.

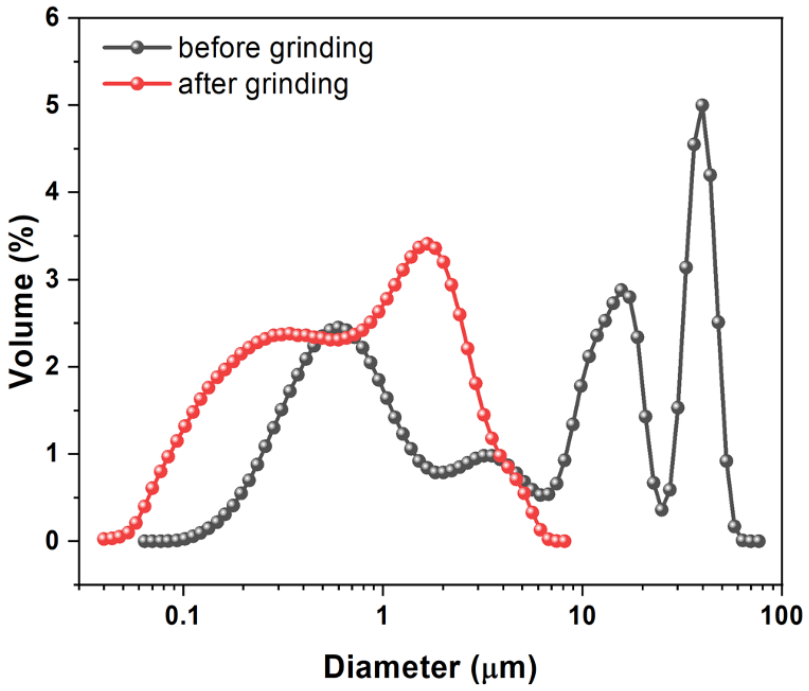

Fig. 2. Particle size distribution for the Al-LLZTO powders before and after grinding by pestle and mortar.

Figure 3 shows XRD patterns of the as-calcined Al-LLZTO powder, and Al-LLZTO disks made from 50wt% and 70wt% Al-LLZTO suspensions by pressure filtration followed by sintering and Al-LLZTO disks made by dry pressing followed by sintering. The samples were sintered at 1100, 1140, and 1180°C, as indicated in the figures. The XRD pattern of cubic garnet $Li_5La_3Nb_2O_{12}$ (Pearson's crystal data card #1237175) is used as a reference for comparing peak positions. Only a cubic garnet phase without impurities was observed in the as-calcined Al-LLZTO powder, and

in the Al-LLZTO disks made from 50 and 70wt% suspensions. However, a series of small shoulder peaks at 2θ of 20, 25, 27, and 30° were found in the XRD patterns of dry-pressed and sintered Al-LLZTO disks. These shoulder peaks indicate that there may be a small amount of the tetragonal garnet phase present in the dry-pressed and sintered disks[10]. In general, the sintering temperature required to obtain the tetragonal garnet phase is lower than that of the cubic garnet phase [21,25]. Our results show that temperature equal to or higher than 1180°C is required for dry-pressed disks to obtain a pure cubic garnet phase. But for disks made by pressure filtration, the sintering temperature can be as low as 1100°C to obtain a pure cubic garnet phase. Figure 3 shows XRD patterns of the as-calcined Al-LLZTO powder, and Al-LLZTO disks made from 50wt% and 70wt% Al-LLZTO suspensions by pressure filtration and sintering and Al-LLZTO disks made by dry pressing and sintering. The samples were sintered at 1100, 1140, and 1180°C, respectively. The XRD patterns of cubic garnet $Li_5La_3Nb_2O_{12}$ (Pearson's crystal data card #1237175) are labeled as a reference. Only a cubic garnet phase without impurities was observed in the as-calcined Al-LLZTO powder, and Al-LLZTO sintered disks made from 50 and 70wt% suspensions. However, a series of small shoulder peaks at 2θ of 20, 25, 27, and 30° can be found in the XRD patterns of dry-pressed and sintered Al-LLZTO disks. These shoulder peaks indicate that there is some tetragonal garnet phase present in the disks made by dry-pressing and sintering [10]. In general, the sintering temperature required to obtain the tetragonal garnet phase is lower than that to obtain the cubic garnet phase [21,25]. Our results show that a sintering temperature equal to or more than 1180°C is required for the disks made by dry-pressing to obtain a pure cubic garnet phase. But for disks made by pressure filtration, the sintering temperature can be as low as 1100°C to obtain a pure cubic garnet phase.

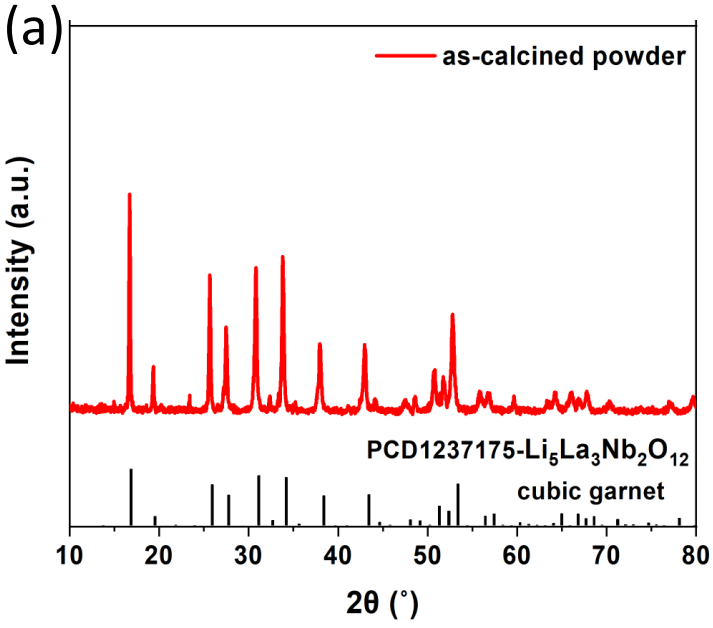
(a)
as-calcined powder
Intensity (a.u.)
PCD1237175-Li5La3Nb2O12
cubic garnet
10
20
30
40
50
60
70
80
2θ (°)

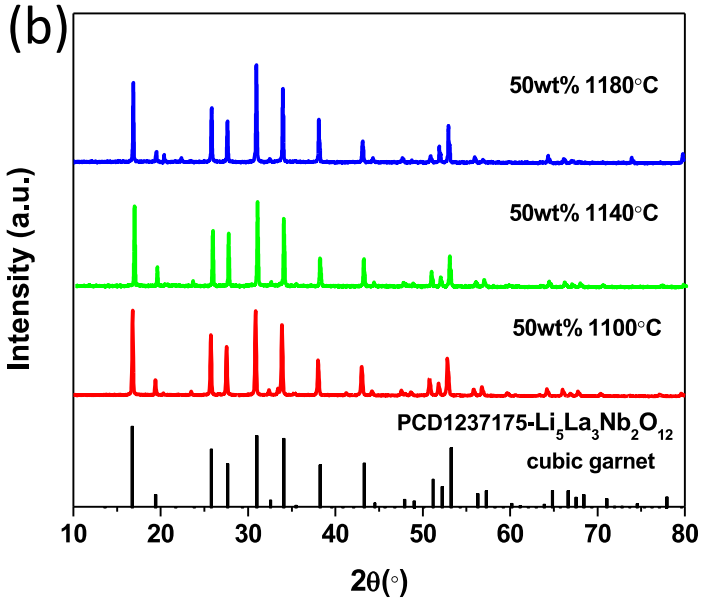
(b)
50wt% 1180°C
50wt% 1140°C
50wt% 1100°C
Intensity (a.u.)
PCD1237175-Li5La3Nb2O12
cubic garnet
10
20
30
40
50
60
70
80
2θ(°)

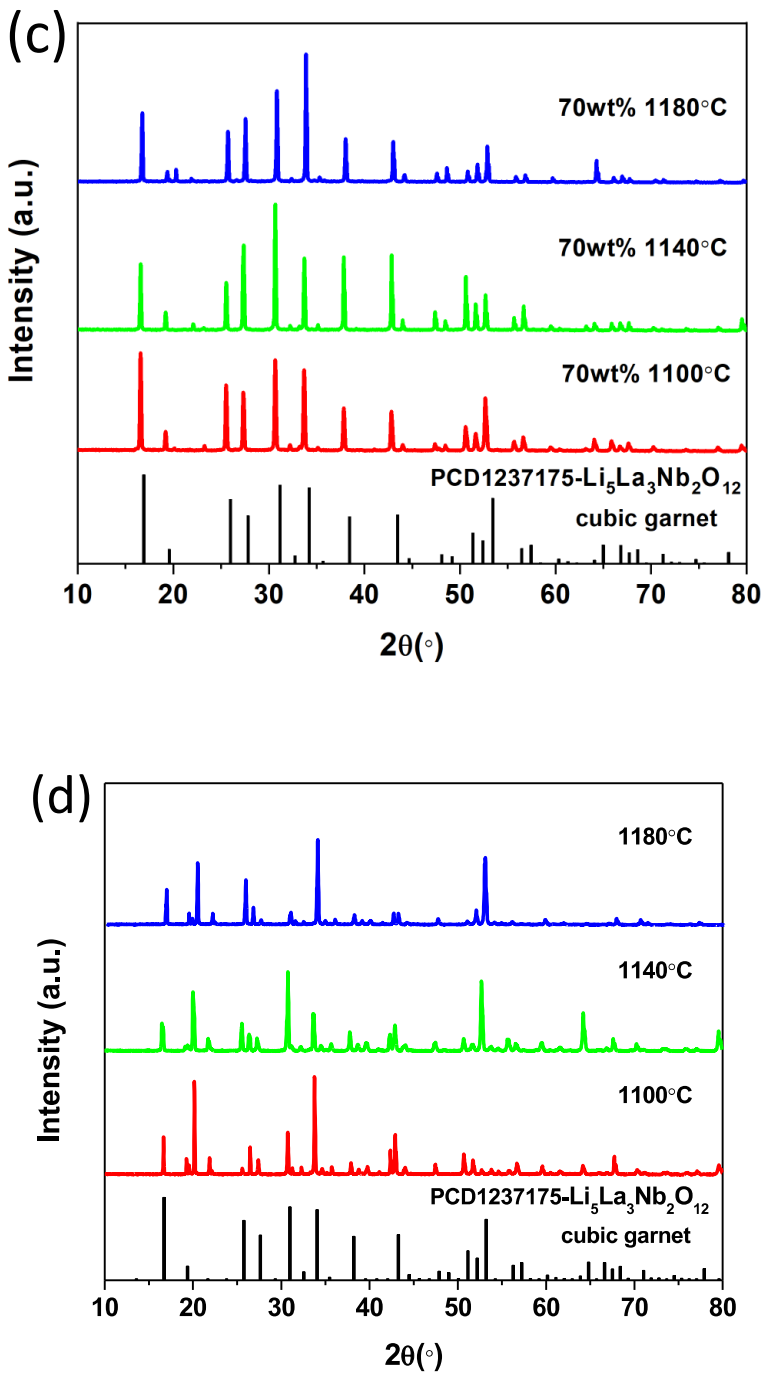

Fig. 3. XRD patterns of (a) as-calcined Al-LLZTO powder, and Al-LLZTO sintered disks made from (b) 50wt% Al-LLZTO suspension by pressure filtration, (c) 70wt% Al-LLZTO suspension by pressure filtration, and (d) Al-LLZTO powders dry-pressed. All disks were sintered at three temperatures: 1100, 1140, and 1180°C.

Figure 4 shows cross-sectional SEM images of the LLZTO sintered disks made from (a-c) 50wt% Al-LLZTO suspension by pressure filtration, (d-f) 70wt% Al-LLZTO suspension by pressure filtration, and (g-i) Al-LLZTO powders by dry pressing, sintered at (a), (d), (g) 1100°C, (b), (e), (h) 1140°C and (c), (f), (i) 1180°C. It is clear that in the sintered disks made by pressure filtration, 1100°C is too low a temperature to form dense samples. The morphologies of Figure 4(a) and 4(d) show that large garnet grains have not formed. However, in sintered disks made dry-pressing Al-LLZTO powder, 1100°C is a high enough temperature to form well-sintered disks. Even though there are some pores residing inside grains, their frequency can be reduced by increasing the sintering temperature. The densities and relative densities are shown in Table 1, which are consistent with the cross-sectional SEM images. The relative densities of the sintered disks made by pressure filtration of the 50wt% Al-LLZTO and the 70wt% Al-LLZTO suspensions sintered at 1100°C are 88% and 85.14%, respectively. The relative density of the sintered disks made dry-pressing sintered at 1100°C is much higher, at 92.57%. The dry weight before density measurement was measured. After density measurement the Al-LLZTO disk surface was wiped dry. The weight increase after density measurement was no greater than 0.17% for all of the Al-LLZTO disks, which shows that there is almost no open connected porosity. Lithium loss during pressure filtration steps may contribute to lower density compared to dry pressing and sintering. When the sintering temperature was increased to 1140°C, garnet grains formed with some closed pores in the sintered disks made by pressure filtration of 50wt% and 70wt% Al-LLZTO suspensions, as seen in Figure 4 (b) and (e), respectively. Also, the relative density increased significantly--90.86% and 92.19% in sintered disks made with 50wt% Al-LLZTO and 70wt% Al-LLZTO suspensions, respectively. The relative densities of the sintered disks made by dry pressing of powders (93.9%) are comparable to those made by pressure filtration disks sintered at 1140°C. In disks made by pressure filtration and sintered at 1180°C, almost pure garnet phase was observed. Also, no pores were observed in the SEM images (Figure 4(c) and (f)). The relative densities of the disks made by pressure filtration and sintered at 1180ºC were 90.66% for 50wt% Al-LLZTO and 93.52% for 70wt% Al-LLZTO. The relative density of the dry-pressed Al-LLZTO disks sintered at 1180°C is as high as 94.67%, but some pores can be seen inside the grains, although less than in samples sintered at lower temperatures (Figure 4(i)). Thus, higher sintering

temperature is required for disks made by both pressure filtration and dry pressing to obtain dense LLZTO disks.

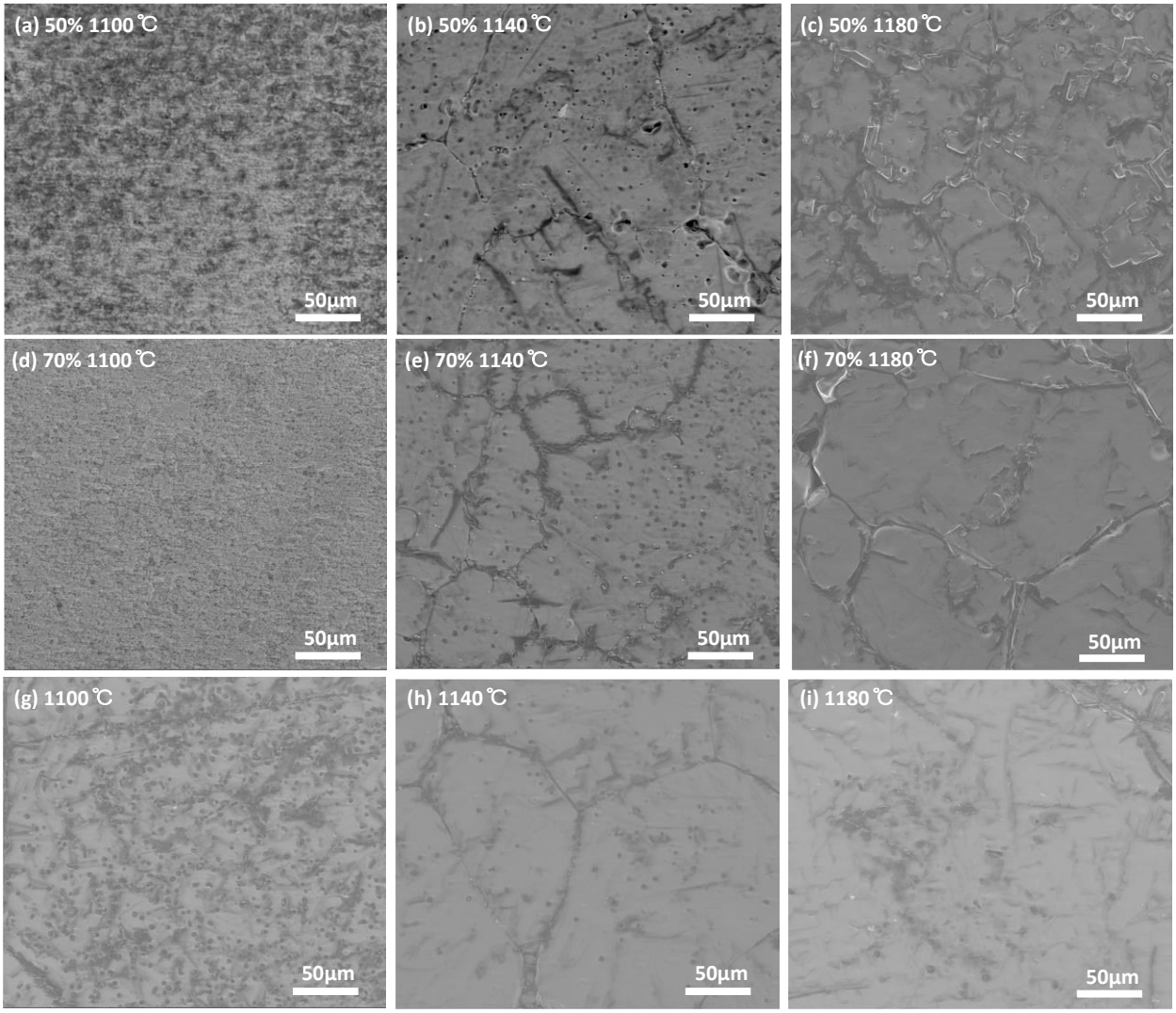

Fig. 4. Cross-section SEM images of LLZTO disks made from either (a-c) 50wt% Al-LLZTO suspension by pressure filtration, (d-f) 70wt% Al-LLZTO suspension by pressure filtration, and (g-i) Al-LLZTO powders by dry pressing, and sintered at (a), (d), (g) 1100°C, (b), (e), (h) 1140°C and (c), (f), (i) 1180°C.

Table 1. Summary of density and relative density for 50%Al-LLZTO and 70% Al-LLZTO pressure filtration disks and Al-LLZTO dry-pressed disks.

Conditions	density g/cm^3	Relative density
50wt% pressure filtration 1100℃	4.62	88.00%
50wt% pressure filtration 1140℃	4.77	90.86%
50wt% pressure filtration 1180℃	4.76	90.67%
70wt% pressure filtration 1100℃	4.47	85.14%
70wt% pressure filtration 1140℃	4.84	92.19%
70wt% pressure filtration 1180℃	4.91	93.52%
Dry pressing 1100℃	4.86	92.57%
Dry pressing 1140℃	4.93	93.90%
Dry pressing 1180℃	4.97	94.67%

Figure 5 shows the impedance spectra of samples over a temperature range from room temperature to 80℃ on LLZTO disks made from 50wt% Al-LLZTO suspension by pressure filtration and sintering (a-c), from 70wt% Al-LLZTO suspension by pressure filtration and sintering (d-f), and from Al-LLZTO powders by dry pressing and sintering, over a sintering temperature range from 1100ºC and 1180ºC. For disks made by 50wt% pressure filtration and sintered at 1100℃ and 1140℃, and for disks made by 70wt% pressure filtration and sintered at 1100℃, clear semicircles and tails can be observed. The minima in the intermediate frequency range were attributed to the Al-LLZTO combined grain and grain boundary resistances. The high frequency intercept on the x-axis is attributed to the AL-LLZTO grain resistance. This assumes that equivalent circuit corresponds to grain resistance, R_g, is in series with a parallel combination of grain boundary resistance, R_{gb}, and grain boundary capacitance, C_{gb}. Thus, at a sufficiently high frequency, the grain boundary resistance is shorted. The corresponding estimated grain conductivity (σ_g) and total conductivity (σ_t), the latter includes both grain and grain boundary contributions, are listed in Table 2. For samples made by pressure filtration and sintering at 1180ºC (50 wt.% suspension) and samples made by pressure filtration and sintering at 1140ºC and 1180ºC (70 wt.% suspension), no semicircular arcs were observed. In samples made by dry pressing and sintering, semicircular arcs were not observed in any of the EIS spectra. In these cases, it is

therefore concluded that grain boundary contributions are negligible. Similar observations were made by Huang et al. [26] in all of Mg-doped lithium garnet samples investigated in their samples. The observation of distinct grain boundary contributions in the present work on samples made by pressure filtration and sintering (1100ºC and 1140ºC for 50 wt.% suspension and 1100ºC for 70 wt.% suspension) may indicate some depletion of lithium that may have occurred during pressure filtration. It appears this depletion probably disappears when sintered at a higher temperature at which uniform distribution of lithium occurs. EIS spectra of samples made by dry-pressing and sintering are shown in Figure 5 (g-i). None of the spectra show semicircular arcs indicating that grain boundary resistance contribution is negligible. The Arrhenius plots of the conductivities are shown in Figure 6 and the activation energies are listed in Table 2. Samples made by pressure filtration and sintering (50 wt.% suspension for 1100ºC and 1140ºC and 70 wt.% suspension for 1100ºC) exhibit lower conductivities and higher activation energies (~0.6 eV) consistent with possible depletion of lithium from grain boundaries. For all other samples, the activation energies are on the order of ~0.3 eV, consistent reported values for similar materials [26, 27]. Since gold paste was used as electrodes, they are blocking to lithium ions. This part thus behaves as an ideally polarized electrode.

Recently, Shen et al.[27] reported a high ionic conductivity of 5.36×10^{-4} S/cm for the $Li_{6.4}La_3Zr_{1.4}Ta_{0.6}O_{12}$ sintered at 1250°C, while Li et al. [28] reported an ionic conductivity of 2.2×10^{-4} S/cm for their $Li_{6.75}La_3Zr_{1.75}Ta_{0.25}O_{12}$ without Li_2O additive sintered at 1230°C. A high Ta doping level was selected by Shen, and a pre-calcination process was used for achieving high density and high ionic conductivity. In contrast, Li et al. [28] used $La(OH)_3$ instead of La_2O_3 as their starting powder, and they did not achieve high ionic conductivity without Li_2O additive. Many factors can contribute to the difference between our results and theirs, such as the starting powders, the particle size, the doping level, the fabrication method, the sintering temperature and the sintering atmosphere. It is not our goal to just compare the ionic conductivity of the LLZTO disk; rather our goal is to obtain samples with high density, good ionic conductivity, and enhance transparency for LLZTO to make high-quality LLZTO disks for further research on lithium dendrite growth. With the exception of samples made by pressure filtration and sintering (1100ºC and 1140ºC for 50 wt.% suspension and 1100ºC for 70wt.% suspension) the conductivity values and activation energies measured in the present work are consistent with values reported in the

literature on similar materials [29–31]. High ionic conductivity and low activation energy Al-LLZTO disks were obtained by pressure filtration and sintering, which demonstrates the pressure filtration does not damage Al-LLZTO.

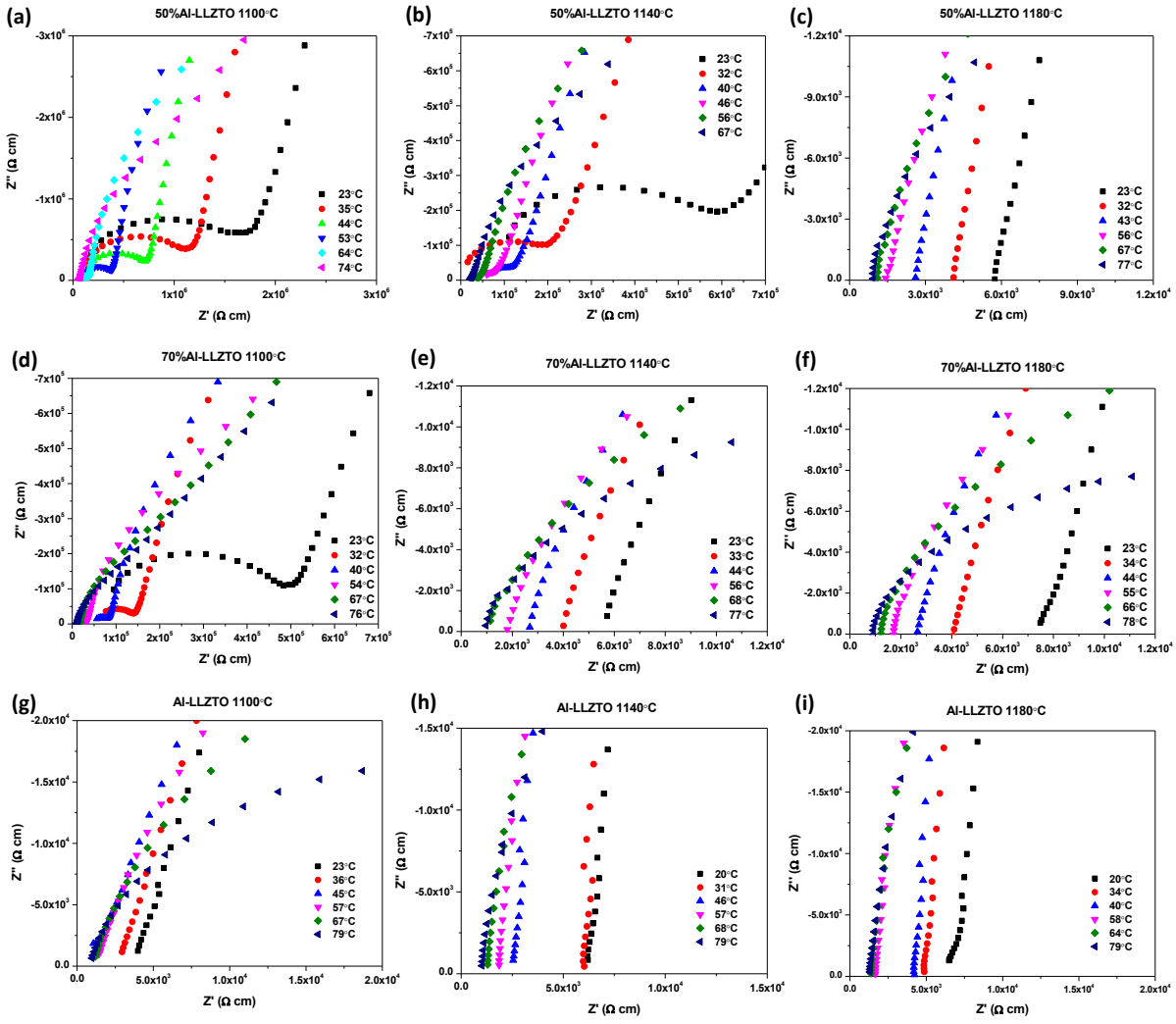

Fig. 5. Impedance spectra at different temperatures for LLZTO disks made from either (a-c) 50wt% Al-LLZTO suspension by pressure filtration, (d-f) 70wt% Al-LLZTO suspension by pressure filtration, and (g-i) Al-LLZTO powders by dry pressing, and sintered at (a), (d), (g) 1100°C, (b), (e), (h) 1140°C and (c), (f), (i) 1180°C.

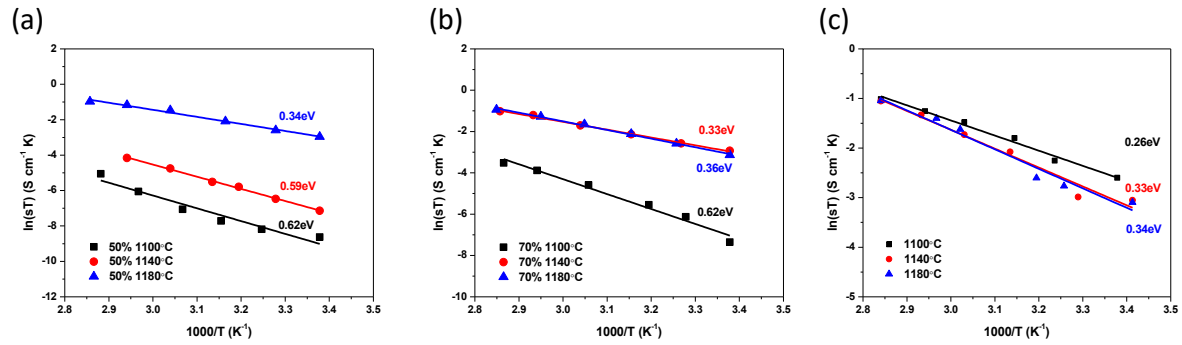

Fig. 6. Arrhenius plots of conductivities for Al-LLZTO disks made by either (a) 50wt% Al-LLZTO suspension by pressure filtration, (b) 70wt% Al-LLZTO suspension by pressure filtration, and (c) Al-LLZTO powders by dry pressing, sintered at 1100, 1140, and 1180°C.

Table 2. Summary of conductivity and activation energy for 50%Al-LLZTO and 70% Al-LLZTO pressure filtration disks and Al-LLZTO dry-pressed disks.

Conditions	Conductivity (S/cm) at room temperature	Activation energy (ev)
50wt% pressure filtration/1100°C	6.05×10^{-7}	0.62
50wt% pressure filtration/1140°C	2.68×10^{-6}	0.59
50wt% pressure filtration/1180°C	1.74×10^{-4}	0.34
70wt% pressure filtration/1100°C	2.16×10^{-6}	0.62
70wt% pressure filtration/1140°C	1.80×10^{-4}	0.33
70wt% pressure filtration/1180°C	1.47×10^{-4}	0.36
Dry pressing 1100°C	2.51×10^{-4}	0.26
Dry pressing 1140°C	1.61×10^{-4}	0.33
Dry pressing 1180°C	1.54×10^{-4}	0.34

Figure 7 shows the UV–vis spectra from 300 to 800 nm of Al-LLZTO made from 50wt% Al-LLZTO suspension by pressure filtration, 70wt% Al-LLZTO suspension by pressure filtration, or

Al-LLZTO powders by dry pressing, sintered at (a) 1100°C, (b) 1140°C and (c) 1180°C. All of the disks were ground down to 0.5mm in thickness, and the surface roughness Rz was controlled to 0-50 μm by polishing to minimize light scattering caused by the surface roughness [32,33]. Al-Neither of the LLZTO disks made by pressure filtration and sintering at 1100ºC exhibits good transparency (see Figure 7(a)). The transmittance of these samples is below 6% from 500 to 800 nm. However, disk dry-pressed and sintered at 1100ºC shows higher transmittance, which is 5-15% from 500 to 800 nm. This is consistent with the SEM results, since the disks made pressure filtration and sintering at 1100ºC were not well-sintered. For Al-LLZTO disks made by pressure filtration and sintering at 1140°C, the transmittance does improve (see Figure 7(b)). However, the transmittance of disks made dry-pressing and sintering doesn't change much. When disks made by pressure filtration using 70wt% suspension and sintering at 1180ºC, the transparency increases to 17-23% for visible light from 500 to 800 nm, which is much higher than the Al-LLZTO disks fabricated by dry pressing and using pressure filtration with 50wt% suspension sintered at the same temperature, Figure 7(c). For comparison, Yang et al. [10] reported an Mg doped LLZO solid electrolyte (thickness 230μm) with low ionic conductivity (5.56×10^{-5} S/cm) prepared by sol-gel, with a transmittance of about 10–12% to visible light from 500 to 800 nm. Thus, pressure filtration and sintering is a good method to obtain transparent LLZTO electrolytes. The high transparency of Al-LLZTO opens new opportunities for studying lithium dendrite growth.

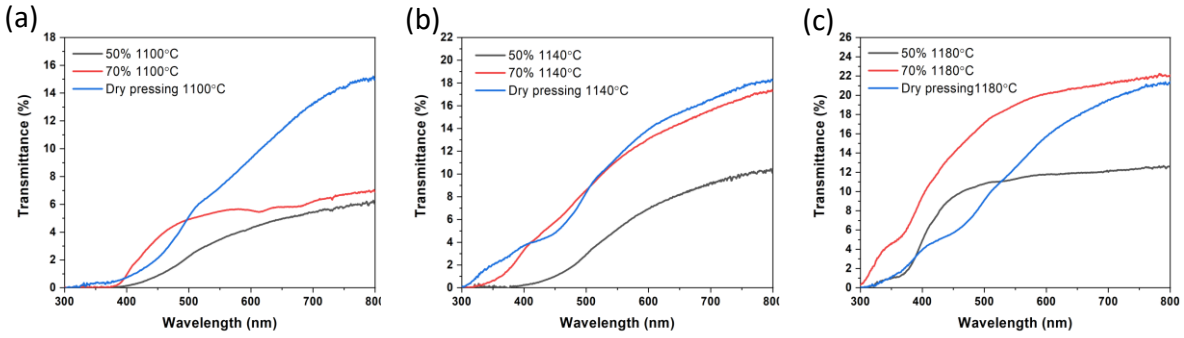

Fig. 7. UV–vis spectrums of Al-LLZTO made from 50wt% Al-LLZTO suspension by pressure filtration, 70wt% Al-LLZTO suspension by pressure filtration, or Al-LLZTO powders by dry pressing, sintered at (a) 1100°C, (b) 1140°C and (c) 1180°C.

Figure 8(a) shows a digital photo of Al-LLZTO disk (thickness 1mm) sintered at 1180°C placed on top of the letter "U" exposed to white light made from 70wt% Al-LLZTO suspension by pressure filtration and sintering. The top view digital photos of the Al-LLZTO disks (thickness 1mm) sintered at 1180ºC made from (b) Al-LLZTO powders by dry pressing, (c) 50wt% Al-LLZTO suspension by pressure filtration, and (d) 70wt% Al-LLZTO suspension by pressure filtration, are also shown in Figure 8. All of the disks were exposed to white light. The sintered disk made by pressure filtration with 70wt% Al-LLZTO suspension clearly exhibits the sharpest "U", demonstrating the improvement in transmittance. A lithium dendrite growth experiment was performed in an argon-filled glove box using the disk made by pressure filtration and sintering at 1180ºC; the testing set-up is shown in Figure 8(e). A lithium wire and a silver wire were placed on the surface of the Al-LLZTO disk; they were connected to a voltage generator. A DC bias was applied for dendrite growth investigation. Figure 8(f) shows the lithium dendrites formed in an Al-LLZTO disk sintered at 1180°C made from 70wt% Al-LLZTO suspension by pressure filtration. The Al-LLZTO disk was in an argon-filled glove box and placed under the microscope. Sharp dendrites can be clearly seen with the light transmitted through. Also, lithium dendrites grew in the Al-LLZTO disk indirectly confirms that the Al-LLZTO disk made by pressure filtration and sintering has a high lithium ionic conductivity.

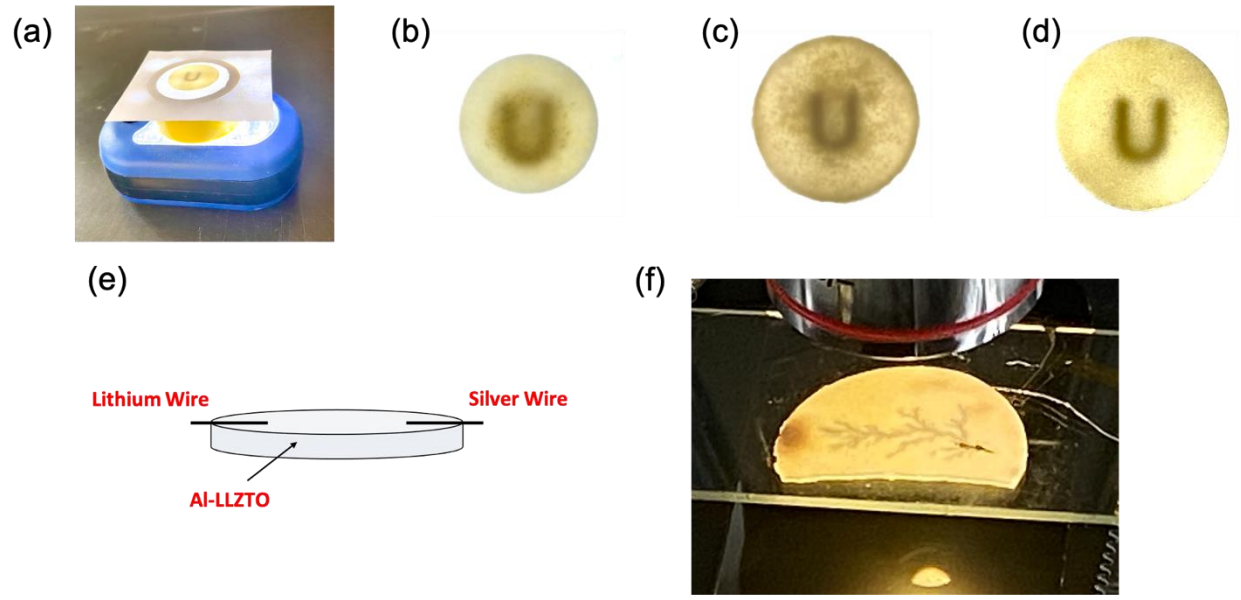

Fig. 8. (a) Digital photo of Al-LLZTO disk sintered at 1180°C exposed to white light made from 70wt% Al-LLZTO suspension by pressure filtration. Top view digital photos of Al-LLZTO disks sintered at 1180°C exposed to white light made from either (b) Al-LLZTO powders by dry pressing, (c) 50wt% Al-LLZTO suspension by pressure filtration, and (d) 70wt% Al-LLZTO suspension by pressure filtration. (e) Schematic set-up for lithium dendrite growth. (f) Digital photo of lithium dendrites in Al-LLZTO disked made from 70wt% Al-LLZTO suspension by pressure filtration sintered at 1180°C.

4. Conclusions

Dense and semi-transparent Al-LLZTO disks with high ionic conductivity were made by pressure filtration and sintering. High density (93.52% theoretical) was achieved using 70wt% Al-LLZTO suspension for pressure filtration followed by sintering. Also, high ionic conductivity (1.47×10^{-4} S/cm) and low activation energy (0.36 eV) were achieved using 70wt% Al-LLZTO pressure suspension and sintered at 1180°C. High transparency with transmittance of 17-23% to visible light from 500 to 800 nm was achieved.

Acknowledgements

This work was supported in part by the National Science Foundation under grant numbers NSF-DMR-1742696, and in part by Department of Energy, Office of Basic Energy Sciences under grant number DE-FG02-03ER46086.

References

[1] Q. Liu, Z. Geng, C. Han, Y. Fu, S. Li, Y. bing He, F. Kang, B. Li, Challenges and perspectives of garnet solid electrolytes for all solid-state lithium batteries, J. Power Sources. 389 (2018) 120–134. https://doi.org/10.1016/j.jpowsour.2018.04.019.

[2] A.M. Nolan, Y. Liu, Y. Mo, Solid-State Chemistries Stable with High-Energy Cathodes for Lithium-Ion Batteries, ACS Energy Lett. (2019) 2444–2451. https://doi.org/10.1021/acsenergylett.9b01703.

[3] F. Zheng, M. Kotobuki, S. Song, M.O. Lai, L. Lu, Review on solid electrolytes for all-solid-state lithium-ion batteries, J. Power Sources. 389 (2018) 198–213. https://doi.org/10.1016/j.jpowsour.2018.04.022.

[4] J. Schnell, T. Günther, T. Knoche, C. Vieider, L. Köhler, A. Just, M. Keller, S. Passerini, G. Reinhart, All-solid-state lithium-ion and lithium metal batteries – paving the way to large-scale production, J. Power Sources. 382 (2018) 160–175. https://doi.org/10.1016/j.jpowsour.2018.02.062.

[5] R. Murugan, V. Thangadurai, W. Weppner, Fast lithium ion conduction in garnet-type Li7La 3Zr2O12, Angew. Chemie - Int. Ed. 46 (2007) 7778–7781. https://doi.org/10.1002/anie.200701144.

[6] M. Huang, T. Liu, Y. Deng, H. Geng, Y. Shen, Y. Lin, C.W. Nan, Effect of sintering temperature on structure and ionic conductivity of Li 7 - XLa 3Zr 2O 12 - 0.5x (x = 0.5 ~ 0.7) ceramics, Solid State Ionics. 204–205 (2011) 41–45. https://doi.org/10.1016/j.ssi.2011.10.003.

[7] J. Awaka, N. Kijima, H. Hayakawa, J. Akimoto, Synthesis and structure analysis of tetragonal Li7La3Zr2O12 with the garnet-related type structure, J. Solid State Chem. 182 (2009) 2046–2052. https://doi.org/10.1016/j.jssc.2009.05.020.

[8] Y. Wang, W. Lai, High ionic conductivity lithium garnet oxides of Li 7-xLa 3Zr 2-xTa xO

12 compositions, Electrochem. Solid-State Lett. 15 (2012) 3–7. https://doi.org/10.1149/2.024205esl.

[9] Y. Ren, H. Deng, R. Chen, Y. Shen, Y. Lin, C.W. Nan, Effects of Li source on microstructure and ionic conductivity of Al-contained Li6.75La3Zr1.75Ta0.25O12 ceramics, J. Eur. Ceram. Soc. 35 (2015) 561–572. https://doi.org/10.1016/j.jeurceramsoc.2014.09.007.

[10] X. Yang, D. Kong, Z. Chen, Y. Sun, Y. Liu, Low-temperature fabrication for transparency Mg doping Li7La3Zr2O12 solid state electrolyte, J. Mater. Sci. Mater. Electron. 29 (2018) 1523–1529. https://doi.org/10.1007/s10854-017-8062-4.

[11] X. Huang, Y. Lu, J. Jin, S. Gu, T. Xiu, Z. Song, M.E. Badding, Z. Wen, Method Using Water-Based Solvent to Prepare Li7La3Zr2O12 Solid Electrolytes, ACS Appl. Mater. Interfaces. 10 (2018) 17147–17155. https://doi.org/10.1021/acsami.8b01961.

[12] S.W. Baek, J.M. Lee, T.Y. Kim, M.S. Song, Y. Park, Garnet related lithium ion conductor processed by spark plasma sintering for all solid state batteries, J. Power Sources. 249 (2014) 197–206. https://doi.org/10.1016/j.jpowsour.2013.10.089.

[13] Y. Li, Z. Wang, C. Li, Y. Cao, X. Guo, Densification and ionic-conduction improvement of lithium garnet solid electrolytes by flowing oxygen sintering, J. Power Sources. 248 (2014) 642–646. https://doi.org/10.1016/j.jpowsour.2013.09.140.

[14] Y. Sun, S. Shimai, X. Peng, G. Zhou, S. Wang, Gelcasting and vacuum sintering of translucent alumina ceramics with high transparency, J. Alloys Compd. 641 (2015) 75–79. https://doi.org/10.1016/j.jallcom.2015.04.026.

[15] H. Chen, S. Shimai, J. Zhao, Z. Di, X. Mao, J. Zhang, J. Liu, G. Zhou, S. Wang, Pressure filtration assisted gel casting in translucent alumina ceramics fabrication, Ceram. Int. 44 (2018) 16572–16576. https://doi.org/10.1016/j.ceramint.2018.06.079.

[16] P. Hip, A. Experimental, Manufacturing of Large Size and Highly Transparent Nd : YAG Ceramics by Pressure Slip-Casting and, (n.d.).

[17] N. Dasgupta, E. Sörge, B. Butler, T.C. Wen, D.K. Shetty, L.R. Cambrea, D.C. Harris, Synthesis and characterization of Al 2-xSc x(WO 4) 3 ceramics for low-expansion infrared-transmitting windows, J. Mater. Sci. 47 (2012) 6286–6296. https://doi.org/10.1007/s10853-012-6548-2.

[18] T.-C. Wen, D.K. Shetty, Colloidal processing and optical transmittance of submicron

polycrystalline alumina, Wind. Dome Technol. Mater. XII. 8016 (2011) 80160C. https://doi.org/10.1117/12.884311.

[19] Y. Hirata, M. Nakamura, M. Miyamoto, Y. Tanaka, X.H. Wang, Colloidal consolidation of ceramic nanoparticles by pressure filtration, J. Am. Ceram. Soc. 89 (2006) 1883–1889. https://doi.org/10.1111/j.1551-2916.2006.01046.x.

[20] Y. Hirata, Y. Tanaka, Pressure filtration model of ceramic nanoparticles, J. Am. Ceram. Soc. 91 (2008) 819–824. https://doi.org/10.1111/j.1551-2916.2007.02204.x.

[21] M. Kotobuki, K. Kanamura, Y. Sato, T. Yoshida, Fabrication of all-solid-state lithium battery with lithium metal anode using Al2O3-added Li7La3Zr 2O12 solid electrolyte, J. Power Sources. 196 (2011) 7750–7754. https://doi.org/10.1016/j.jpowsour.2011.04.047.

[22] T.-C. Wen, Effect of grain size on optical transmittance of birefringent polycrystalline ceramics, University of Utah, 2016.

[23] R. Apetz, M.P.B. Van Bruggen, Transparent Alumina : A Light-Scattering Model, 86 (2003) 480–486.

[24] A. Krell, P. Blank, H. Ma, T. Hutzler, M.P.B. Van Bruggen, R. Apetz, Transparent sintered corundum with high hardness and strength, J. Am. Ceram. Soc. 86 (2003) 12–18. https://doi.org/10.1111/j.1151-2916.2003.tb03270.x.

[25] N. Janani, C. Deviannapoorani, L. Dhivya, R. Murugan, Influence of sintering additives on densification and Li+ conductivity of Al doped Li7La3Zr2O12 lithium garnet, RSC Adv. 4 (2014) 51228–51238. https://doi.org/10.1039/c4ra08674k.

[26] X. Huang, C. Liu, Y. Lu, T. Xiu, J. Jin, M.E. Badding, Z. Wen, A Li-Garnet composite ceramic electrolyte and its solid-state Li-S battery, J. Power Sources. 382 (2018) 190–197. https://doi.org/10.1016/j.jpowsour.2017.11.074.

[27] F. Shen, W. Guo, D. Zeng, Z. Sun, J. Gao, J. Li, B. Zhao, B. He, X. Han, A Simple and Highly Efficient Method toward High-Density Garnet-Type LLZTO Solid-State Electrolyte, ACS Appl. Mater. Interfaces. 12 (2020) 30313–30319. https://doi.org/10.1021/acsami.0c04850.

[28] Y. Li, Y. Cao, X. Guo, Influence of lithium oxide additives on densification and ionic conductivity of garnet-type Li6.75La3Zr 1.75Ta0.25O12 solid electrolytes, Solid State Ionics. 253 (2013) 76–80. https://doi.org/10.1016/j.ssi.2013.09.005.

[29] J.L. Allen, J. Wolfenstine, E. Rangasamy, J. Sakamoto, Effect of substitution (Ta, Al, Ga)

on the conductivity of Li 7La 3Zr 2O 12, J. Power Sources. 206 (2012) 315–319. https://doi.org/10.1016/j.jpowsour.2012.01.131.

[30] X. Zhang, T.-S. Oh, J.W. Fergus, Densification of Ta-Doped Garnet-Type Li 6.75 La 3 Zr 1.75 Ta 0.25 O 12 Solid Electrolyte Materials by Sintering in a Lithium-Rich Air Atmosphere , J. Electrochem. Soc. 166 (2019) A3753–A3759. https://doi.org/10.1149/2.1031915jes.

[31] Y. Cao, Y.Q. Li, X.X. Guo, Densification and lithium ion conductivity of garnet-type Li 7-xLa3Zr2-xTaxO12 (x = 0.25) solid electrolytes, Chinese Phys. B. 22 (2013) 2–7. https://doi.org/10.1088/1674-1056/22/7/078201.

[32] T.-C. Wen, D.K. Shetty, Birefringence and grain-size effects on optical transmittance of polycrystalline magnesium fluoride, Wind. Dome Technol. Mater. XI. 7302 (2009) 73020Z. https://doi.org/10.1117/12.818933.

[33] T.C. Wen, D.K. Shetty, On the effect of birefringence on light transmission in polycrystalline magnesium fluoride, J. Am. Ceram. Soc. 98 (2015) 829–837. https://doi.org/10.1111/jace.13351.